Hindawi
Geofluids
Volume 2021, Article ID 6684884, 11 pages
https://doi.org/10.1155/2021/6684884

Research Article

Field Tests on the Stress Characteristics of Enriched Water Tunnel Invert

Mingqing Du,[1] Xiang Li,[2] Xuchun Wang,[1] Hongwei Teng,[1] Peng Zhang,[1] and Zhen Zhu[1]

[1]*School of Civil Engineering, Qingdao University of Technology, Qingdao, Shandong 266033, China*
[2]*Qingdao Conson Construction and Investment Co., Ltd., Qingdao, Shandong 266000, China*

Correspondence should be addressed to Zhen Zhu; zhuzhen@qut.edu.cn

Received 24 December 2020; Revised 7 January 2021; Accepted 13 January 2021; Published 23 January 2021

Academic Editor: Feng Xiong

To monitor the changes in the force of the tunnel invert steel bars after the groundwater level changes, field tests were performed to accurately and comprehensively characterize the stress acting on the rebar of a tunnel invert. Changes in stress and temperature were monitored for two layers of rebar (upper and lower) in an actual tunnel invert during its repair. The results showed that the changes in stress followed different paths for the upper and lower layers. After the groundwater is replenished, the maximum tensile stress of the rebar was 17.3 MPa, and the maximum compressive stress was 120 MPa. Major changes in stress were observed 2–6 days after rain. Based on this, the seepage path of groundwater is analyzed. During this period, the compressive stress increased threefold, and the tensile stress increased 9.5-fold. The rebar stress in the tunnel invert followed a Gaussian distribution after stabilizing. Four phases of stress progression are identified and discussed. The results can provide data support and theoretical basis for the treatment of invert floor heave in enriched water tunnel.

1. Introduction

In recent years, the construction of high-speed railway has been accelerating. Especially in China, the mileage of high-speed railway has exceeded 35,000 km, which includes a large number of tunnels. An invert is an important part of a tunnel; its force and deformation directly determine whether a high-speed train can run safely and smoothly within the tunnel. Excessive force on the rebar is an important factor for invert floor heave; the change of groundwater level affects the force of invert. Problems with inverts have been widely reported in operational tunnels [1–3]. Thus, many studies have focused on the tunnel structure and surrounding rock failure. Tan et al. based on the Wangjing tunnel project studied the segment displacement and mechanical response of the shield tunnel with a diameter of 10.5 m in the process of shield construction and cross-passage construction [4]. Fang et al. and Zhang et al. calculated the seepage-induced effective stress around a tunnel in an elastic half-plane [5–7]. Li et al. defined a parameter called the partial failure ratio to describe the range of partial failure, which they used to analyze the limit support pressure and failure zone. Numerical simulations showed that their proposed model is very precise [8, 9]. Wen et al. established a flow-stress-damage model and its criterion of fracture expansion [10–12]. Li et al. carried out shear tests and sealed leakage tests on single fracture chlorite schist with or without grouting and evaluated strength and permeability of grouting effect [13–15].

Chiaia et al. introduced a suitable block model for evaluating the crack width and crack spacing of concrete structures with steel bars, which they extended to the serviceability stage of tunnel linings [16]. Kaya and Bulut applied a convergence confinement technique to check the capacity of suggested support units and used the 2D and 3D numerical finite element methods to determine the efficiency of the support design, dimensions of the plastic zones, and deformation [17]. Hu et al. studied the mechanical behavior of tunnel linings and found that the maximum positive bending moment and tensile cracks on the lining mainly develop in the direction normal to stratification [18]. Yoon et al. studied the

(a) (b)

Figure 1: Tunnel cracks: (a) longitudinal and (b) transverse.

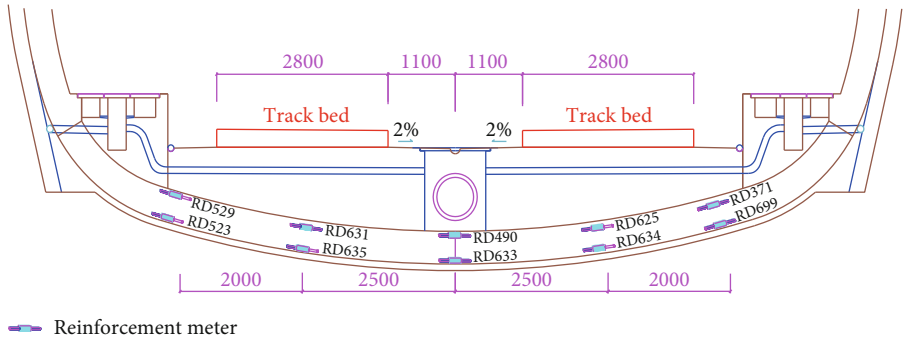

(a)

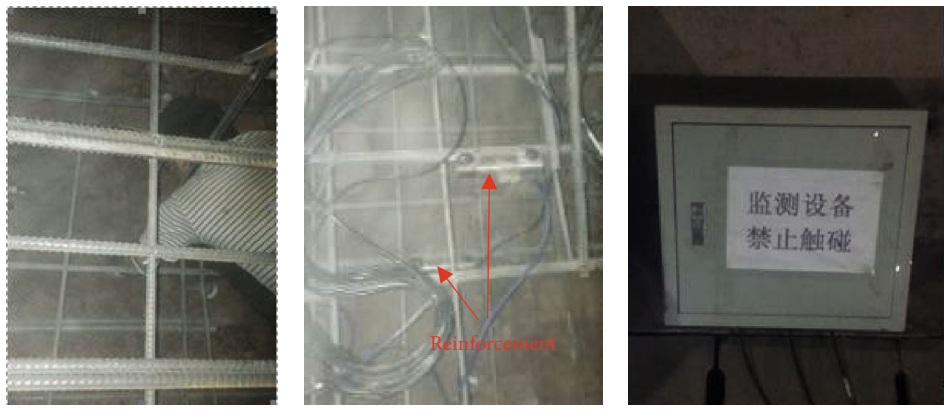

(b) (c) (d)

Figure 2: Field test characteristics: (a) locations of reinforcement meters (cm), (b) installation of extensometers, (c) installed extensometers, and (d) equipment box at the site.

effects of tunnel shapes on structural and hydraulic interactions and proposed a method for evaluating pore water pressure on tunnel linings [19]. Nematollahi and Dias used a finite difference code and nonlinear perfectly plastic constitutive model to study the structural forces induced on a tunnel lining [20]. Nogales et al. studied the mechanical properties of fiber-reinforced concrete in a tunnel lining [21, 22]. Meng et al. presented a novel 3D SRM mesoscale modeling method with concave particles and verified by experimental results [23–25].

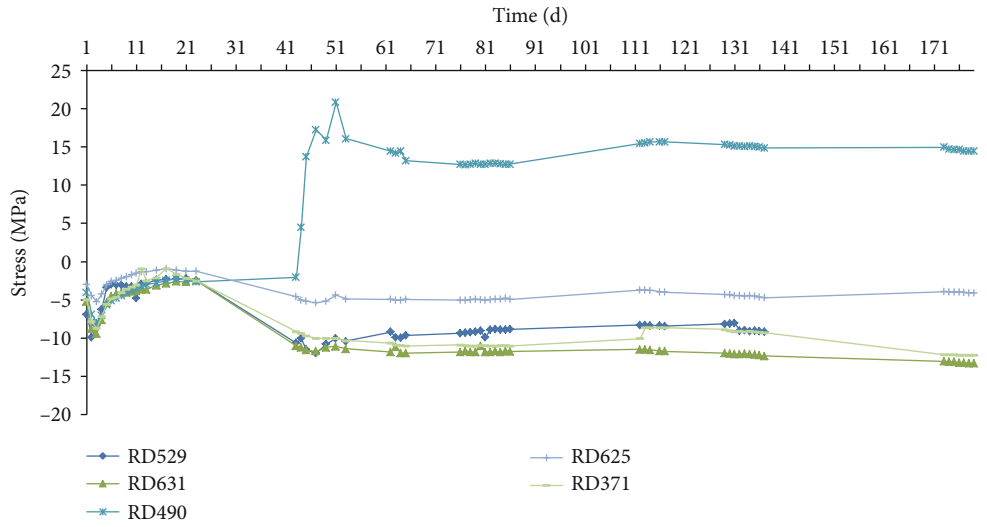

(a)

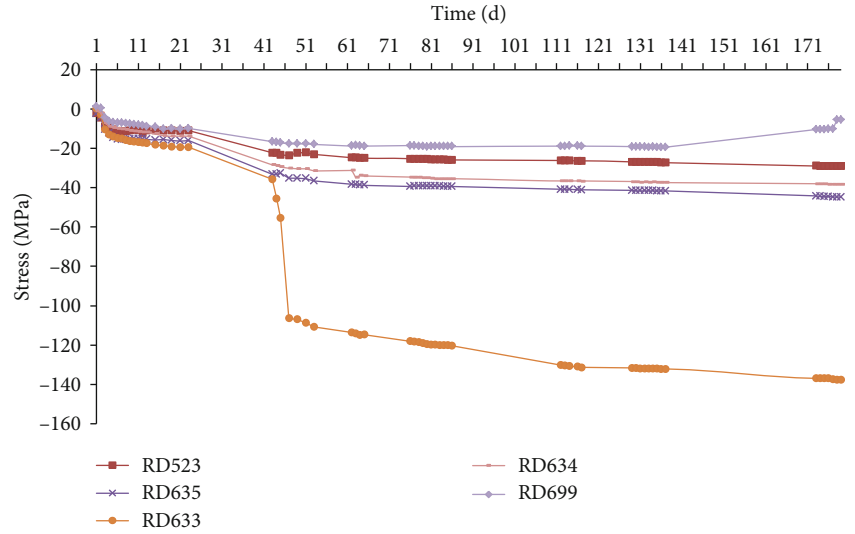

(b)

Figure 3: Continued.

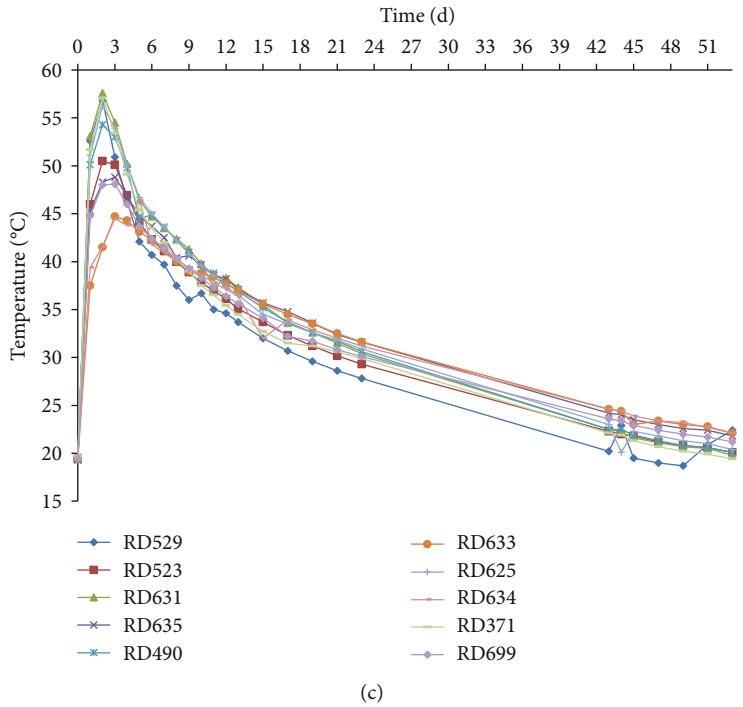

(c)

Figure 3: Field data: (a) stress-time curve for the upper layer of rebar, (b) stress-time curve for the lower layer of rebar, and (c) temperature-time curve.

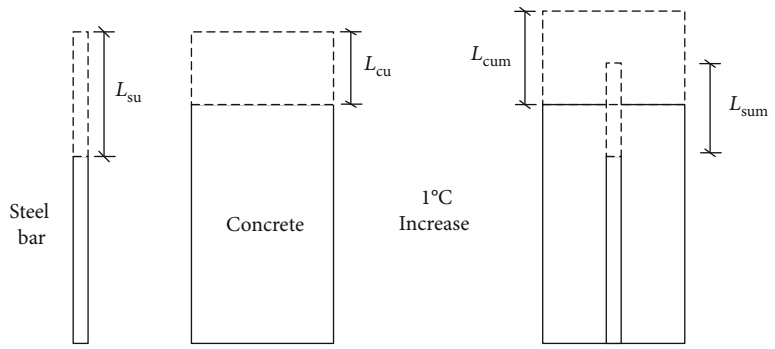

Figure 4: Changes in structure with increasing temperature.

Mou et al. studied 2D and 3D beam-column joints under pseudostatic loadings to investigate the influence of the loading type on seismic behavior, especially regarding the failure mode [26, 27]. Uenishi analyzed the scattering of a plane harmonic body wave by a uniformly lined circular tunnel and evaluated the possible mechanical characteristics of related incident seismic waves according to the failure mode of the structure [28]. Lv et al. and Huang et al. proposed stochastic damage models based on the micromechanical method for the bond stress-slip relationship of the interface under a monotonic load [29, 30]. Lin et al. studied reinforcement corroded to different levels and repeatedly loaded at different stress levels; their results showed that the bond behavior under cyclic loading is characterized by a progressive rise in the residual slip [31]. Campione et al. analyzed the experimental results of the local bond stress-slip relationship for

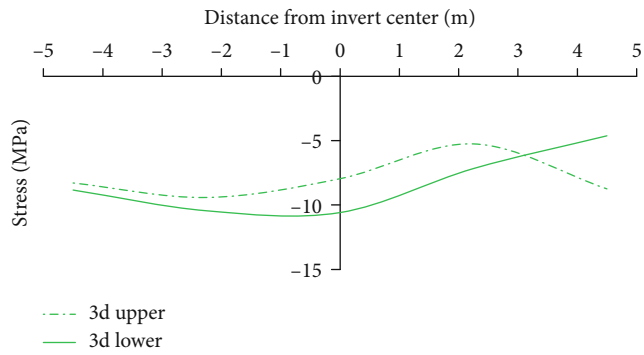

Figure 5: Stress on rebar on day 3.

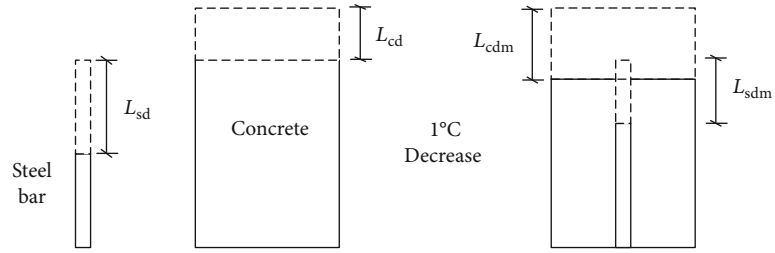

Figure 6: Changes in structure with decreasing temperature.

steel bars embedded in lightweight fiber-reinforced concrete [32]. Xiao et al. analyzed the bond strength between recycled concrete and rebar and proposed a relationship between the stress and slip [33]. Wang et al. performed the pull-out test on 120 specimens; based on the results, they proposed a bond-slip constitutive model and a formula to represent the dissipated energy and elastic deformation energy [34].

Zhu et al. analyzed the effect of water-rock circulation on the mechanical properties of rock through a combination of macromechanical experiments and microstructure tests in the laboratory [35–39]. Zhang et al. performed laboratory tests and theoretical calculations to monitor a tunnel invert and clarified the definition and expression for the bearing capacity of a concrete-filled steel tube (CFST) supporting arch [40]. Kim et al. used laboratory tests and numerical analyses to study the behavior of a tunnel invert in weathered rock [41]. Seki et al. performed model experiments and numerical analysis to establish a rational measure of the heaving phenomenon [42]. Many other researchers have studied the mechanical characteristics and failure process of tunnel inverts through numerical analyses and experimental tests [43–47]. However, most research on inverts has only focused on the ultimate mechanical characteristics of the rebar. The process of changes in stress has been ignored, which is mainly because of the lack of data on the processes by which forces change. As an essential component of the invert structure, the rebar works with the concrete to bear the tensile stress of the invert and compensate for the low tensile strength of the concrete. Thoroughly understanding the stress characteristics and process of the reinforcement is very important for understanding the failure process and mechanism of the invert.

In this study, long-term field monitoring was carried out on the stress of the rebar in the invert of Fuchuan Tunnel of the Lanzhou–Urumqi High-Speed Railway. Meters were installed in the upper and lower rows of the rebar to obtain the changes in stress and temperature throughout the construction process from binding and concrete pouring to tunnel operation. The relationship between the rise of the groundwater level and the force of the invert was studied. The stress of the rebar was divided into four main phases to which different deformation control measures can be applied. This improves upon the current situation, where only the ultimate stress state is considered. The findings of this study will provide data and theoretical support for the deformation control of enriched water tunnel inverts.

2. Field Tests

2.1. General Situation. The invert at the DK41+410 section of Fuchuan Tunnel along the Lanzhou–Urumqi High-Speed Railway was chosen for the field test. Fuchuan Tunnel is in Gansu Province and has a total length of 10.65 km, maximum width of 14 m, and maximum height of 12.7 m. The invert has a concrete thickness of 55 cm and two rows of rebar. During the construction and operation of the tunnel, a large number of cracks appeared in the invert, as shown in Figures 1(a) and 1(b), which seriously affected the safe operation of trains. To accurately understand the internal stress of the invert, sensors were arranged on the rebar to monitor changes in stress as the tunnel was repaired. VWR-22 vibrating string extensometers, which can measure stress in the range of -200 to +300 MPa and temperature in the range of -40 to +150°C, were embedded in the upper and lower rebar layers of the invert directly below the center of the arch and slab track, as shown in Figure 2(a). Five points were monitored in each rebar layer, as shown in Figures 2(b)–2(d).

2.2. Analysis of the Test Results. Figure 3 graphs the stress and temperature of the rebar in the tunnel invert over time. Figure 3(a) shows the stress curve for the upper layer. The five monitoring points initially exhibited similar trends but diverged over time. The compressive stress initially decreased before increasing. Later, tensile stress appeared at the center of the invert and increased continuously, while the other four monitoring points showed that the compressive stress started increasing again. Figure 3(b) shows the corresponding curves for the lower layer. The compressive stress at the five monitoring points increased over time from concrete pouring to actual operation. Figure 3(c) plots the changes in temperature for the rebar. A large amount of hydrated heat was released after the concrete pouring, which caused the temperature of the material to initially increase before returning to room temperature. The rise and fall in temperature directly affected the compressive stress on the rebar. The field test data showed four distinct phases for the rebar in the tunnel invert from concrete pouring to actual operation: (1) the stress increased monotonically; (2) the compressive stress initially decreased before increasing for the upper layer and increased monotonically for the lower layer; (3) the tensile stress increased sharply for both the upper and lower layers; and (4) both the tensile and compressive stresses stabilized.

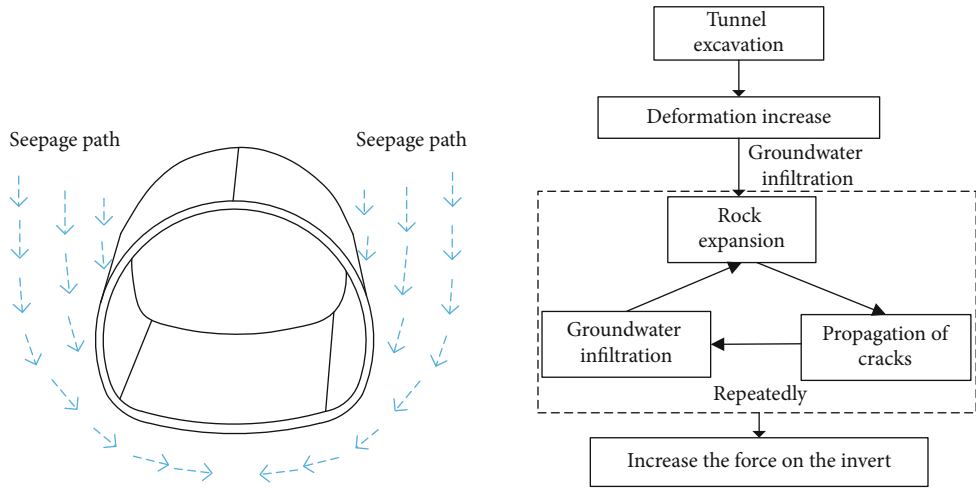

Figure 7: Seepage path and rock expansion process.

2.2.1. Phase 1. In Phase 1, the stress increased monotonically. The stress on the rebar was mainly impacted by the weight of the freshly poured concrete and increase in temperature. The concrete pouring released a large amount of hydration heat, which caused the internal temperature of the concrete to rise. The coefficients of thermal expansion for rebar and concrete are approximately $1.2 \times 10^{-5}{}^{\circ}\mathrm{C}^{-1}$ and $8 \times 10^{-6}{}^{\circ}\mathrm{C}^{-1}$, respectively, which means that the former is more temperature-sensitive than the latter. Consider the case where concrete is not added to rebar, and let L_{su} and L_{cu} be the elongations of the rebar and concrete, respectively, for every 1°C increase in temperature. If rebar is added into concrete, the same 1°C increase in temperature would cause the elongation of the rebar to be constrained by the concrete because the former is larger in magnitude than the latter. In this case, the actual elongation of the rebar (L_{sum}) will be smaller than L_{su}, while the elongation of the concrete (L_{cum}) will be greater than L_{cu}. Hence, the rebar is compressed by $L_{su} - L_{sum}$, which results in compressive stress. Meanwhile, the concrete is elongated by $L_{cum} - L_{cu}$, which results in tensile stress (Figure 4). This phase lasted for roughly 1–3 days. As the temperature increased (Figure 3(c)), the compressive stress on the rebar increased significantly. Figure 5 plots the stress on the rebar distributed horizontally along the tunnel on day 3. On this day, both the upper and lower layers of the rebar experienced compressive stress. This stress reached a maximum at the center of the inverted arch of the tunnel for the lower layer, but this phenomenon did not occur in the upper layer. This may be explained by the uneven distribution of the concrete weight and temperature stress.

2.2.2. Phase 2. In Phase 2, the compressive stress first decreased before increasing for the upper layer and increased monotonically for the lower layer. There were two main contributing factors: the temperature stress and pressure from the surrounding rock. In this phase, the internal temperature of the concrete began to decrease. Let L_{sd} and L_{cd} represent the compressions of the rebar and concrete, respectively, for every 1°C decrease in temperature prior to the rebar being placed in concrete. After the rebar is placed in the concrete,

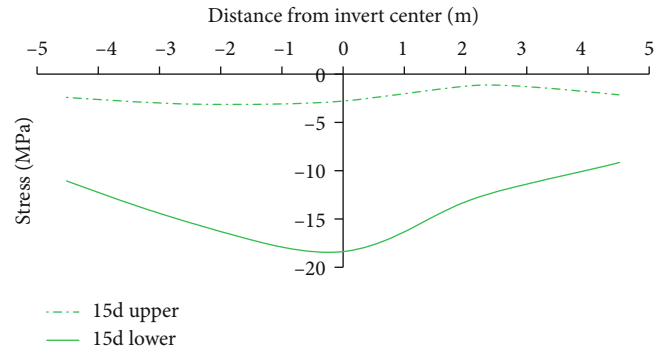

Figure 8: Stress on rebar on day 15.

the compression of the former is constrained by the latter. This also causes the actual compression of the rebar (L_{sdm}) to be less than L_{sd}, so the rebar is impacted by the tensile stress generated by the concrete. This is equivalent to a tensile strain equal to $L_{sd} - L_{sdm}$ acting on the rebar. The concrete is also affected by compressive stress generated from the rebar, which is equivalent to a compressive strain of $L_{cdm} - L_{cd}$ (Figure 6). Hence, the compressive stress on the upper layer of the rebar decreased gradually. Although the compressive stress did not decrease for the lower layer, there was a reduction in its rate of increase. This was mainly caused by the increase in stress on the rebar generated by the surrounding rock while the fall in temperature reduced the compressive stress on the rebar. This indicates that the compressive stress from the surrounding rock had a greater effect than the temperature stress on the lower layer of the rebar.

The field data for the early phases revealed that the free swell ratio of the surrounding rock was greater than 50% (i.e., swelling rock). Groundwater seeped into the rock surrounding the tunnel through cracks, which caused the rock to expand. This compressed both the tunnel invert and unexpanded rock, which created cracks in the unexpanded rock for more groundwater to seep in. The unexpanded rock then absorbed this groundwater, which in turn compressed the tunnel invert and other unexpanded rock. This cycle

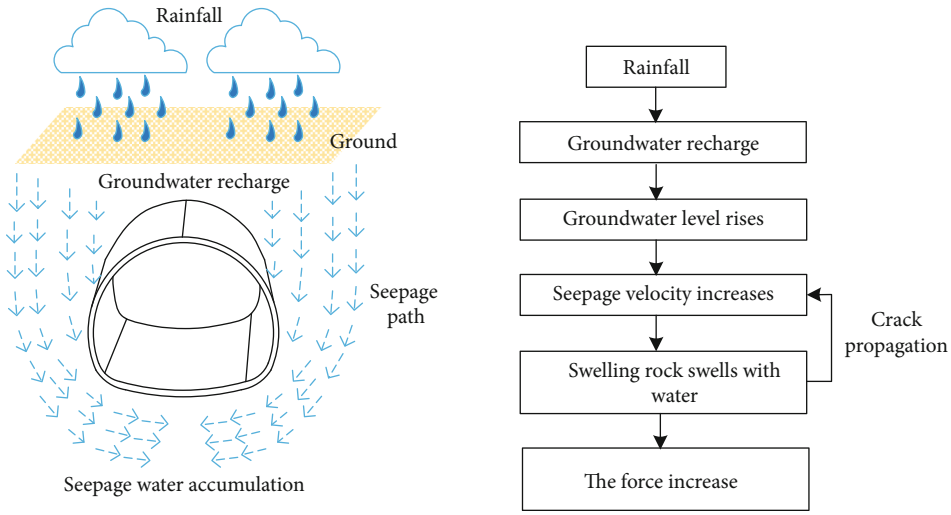

Figure 9: Process for increasing stress from the seepage water accumulation.

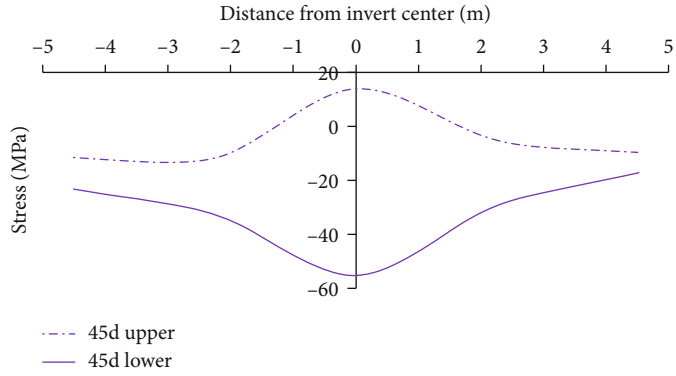

Figure 10: Stress on rebar on day 45.

continued, which caused the lift on the tunnel invert to gradually increase (Figure 7). This in turn created the trend of increasing compressive stress on the lower rebar layer. Phase 2 lasted roughly from day 3 to day 15. Figure 8 shows the stress on the rebar horizontally distributed along the tunnel on day 15. Compared to day 3, the compressive stress on the upper layer decreased significantly while that on the lower layer increased somewhat to a maximum of 18.3 MPa. The compressive stress remained greatest at the center of the tunnel invert, which was mainly due to the expansion of swelling rock caused by groundwater seepage.

2.2.3. Phase 3. In Phase 3, the tensile stress increased sharply for both the upper and lower layers. The data showed that sustained rainfall (>12 h) occurred on day 42. The surrounding rock expanded sharply because of the large amount of rainwater seepage, which rapidly increased the lift on the tunnel invert (Figure 9). This compressed the lower part of the invert and stretched the upper part. This increased the compressive stress on the upper rebar and the tensile stress on the lower rebar. Figure 10 plots the stresses on rebar distributed horizontally across the tunnel on day 45. The tensile stress on the upper layer was the greatest at the center of the invert (13.8 MPa). Similarly, the compressive stress on the lower layer was the greatest at the same location (55.4 MPa) and was roughly 300% greater than the 18.3 MPa observed on day 15. Two to six days after the rain (i.e., days 43–47), the maximum compressive stress on the lower rebar of the invert increased from 35.7 MPa to 106.5 MPa. The stress on the upper rebar changed from a compressive stress of 2 MPa to a tensile stress of 17.3 MPa. In 5 days, the compressive stress increased threefold, and the tensile stress increased 9.5-fold. This indicates that the expansion of the surrounding rock was the main reason for the change in stress on the rebar.

Because of the rapid increase in tensile stress on the rebar, the tensile stress exceeded the tensile strength of the concrete, and cracks began to appear in the concrete. For sections where cracks appeared, the concrete withdrew from tension work, which was transferred to the rebar. This significantly increased the tensile stress. At locations away from the crack, the stresses on the rebar and concrete were redistributed. The stress on the rebar gradually decreased, and the stress on the concrete gradually increased to the tensile strength. When the load increased, secondary cracks appeared at other weak points. As the load increased, new cracks appeared until the structure was damaged.

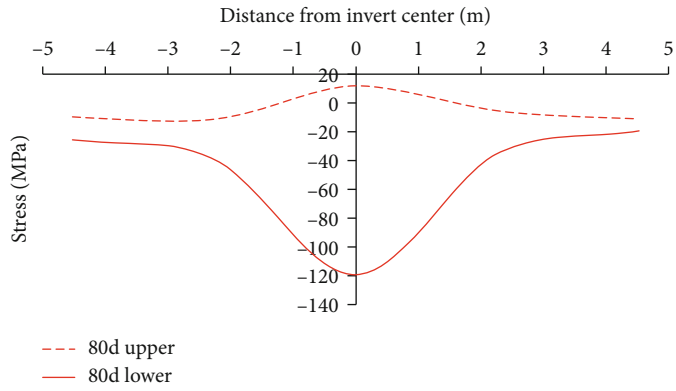

Figure 11: Stress on rebar on day 45.

Table 1: Fitting formulas.

Fitting formula	Adj. R^2
$y = -10.5214 + \left(64.7347/\left(2.0557\sqrt{\pi/2}\right)\right) \exp\left[-2(x-0.4)^2/2.0557^2\right]$	0.9765
$y = -22.3641 + \left(-282.9771/\left(2.3147\sqrt{\pi/2}\right)\right) \exp\left[-2(x+0.0829)^2/2.3147^2\right]$	0.9888

2.2.4. Phase 4. In Phase 4, the stresses generated by the surrounding rock and groundwater had become stable, and the drag of the invert and external lift had roughly evened out. This caused the compressive and tensile stresses acting on the rebar to stabilize. Figure 11 plots the forces acting on the upper and lower layers of the rebar distributed horizontally along the tunnel. The compressive stress on the lower layer was the greatest at the center of the invert structure at roughly 119.7 MPa. This is a 12.4% increase over the stress on day 47 (roughly 106.5 MPa). Curve fitting showed that the stress on the rebar followed a Gaussian distribution. Table 1 presents the curve fitting formulas.

3. Discussion

The field data revealed that the process by which the rebar of a tunnel invert experiences stress is extremely complex and can be divided into four phases. In Phase 1, the stress on both the upper and lower layers of the rebar increased because of the concrete weight and increase in temperature from the hydration heat released during concrete pouring. When the concrete was poured, its weight acted directly on the rebar. This forced the rebar to settle vertically and compressed the upper and lower layers. After the concrete was poured, a large amount of hydration heat was released, and the concrete and rebar expanded thermally. However, the larger expansion coefficient of steel meant that the elongation of the rebar was constrained by its bond with the concrete, which placed the rebar under compressive stress. In Phase 2, the temperature began to decrease, and groundwater gradually converges towards the bottom of the tunnel, causing the surrounding rock to expand and the stress from the surrounding rock gradually increased. The temperature and surrounding rock had counteracting effects on the stress on the rebar. On the one hand, the hydration heat of the concrete was basically released, so the internal temperature of the concrete began to decrease. The bond between the rebar and concrete reduced the shrinkage of the rebar and caused it to be stretched, so the compressive stress on the rebar was reduced. On the other hand, the concrete realized certain strength and could resist part of the stress from the surrounding rock. Groundwater enters the bottom of the tunnel invert through seepage, causing the swelling rock at the bottom to absorb water and expand, and the expansion force directly acts on the tunnel lining structure; this helped increase the stress on the rebar. In Phase 3, the surrounding rock expanded mainly as a result of increased groundwater from continuous rainfall. The swelling of the surrounding rock expanded cracks that let more groundwater in. This sharply increased the lift acting on the invert and made it into a single-span statically indeterminate structure. This increased both the tensile stress acting on the upper layer of the rebar and the compressive stress acting on the lower layer of the rebar at the center of the invert. In Phase 4, the stresses from both the surrounding rock and temperature were largely stable. Because it was winter, the internal temperature of the concrete gradually decreased. However, the temperature decrease was limited, and the resulting temperature stress was negligible compared to the stress from the surrounding rock at this time. Therefore, the stress on the rebar gradually stabilized. This process is shown in Figure 12. Based on the four observed phases, the changes in the forces acting on the tunnel invert were deduced. This can be used to develop different measures for treating floor heave according to the phase, rather than according to the maximum stress. This will allow the floor heave of a tunnel invert to be controlled more accurately.

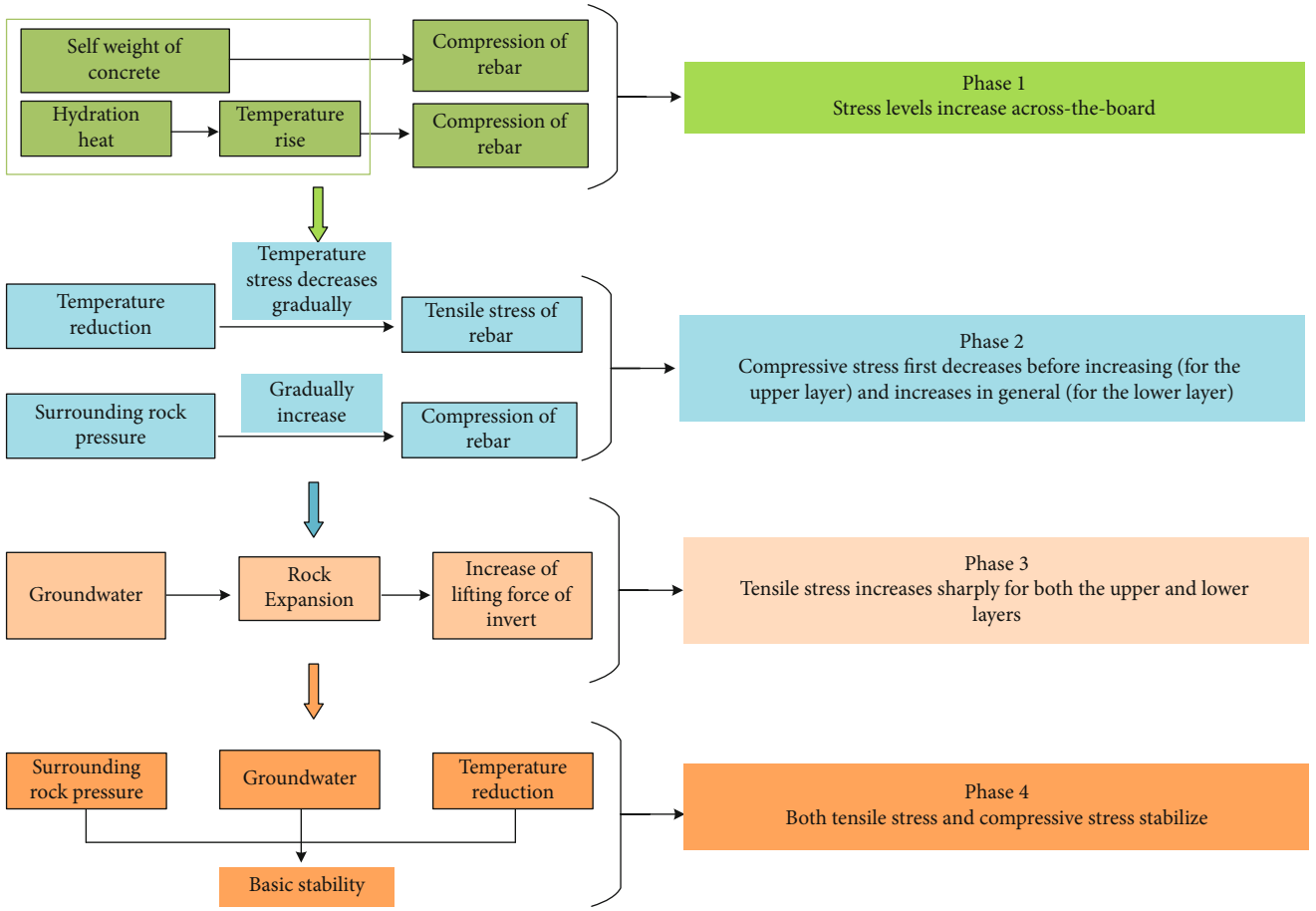

Figure 12: Process for how compressive stress acts on rebar in enriched water tunnel invert.

4. Conclusion

Field tests were performed to obtain the process by which stress acts on the rebar of an enriched water tunnel invert. This will provide data and theoretical support for the rational treatment of floor heave of enriched water tunnel invert. The main conclusions are as follows:

(1) The stress on the rebar in a tunnel invert is extremely complex and can be divided into four major phases: (1) the stress increases monotonically; (2) the compressive stress initially decreases before increasing for the upper layer of the rebar and increases monotonically for the lower layer; (3) the tensile stress increases sharply for both the upper and lower layers; and (4) both the tensile and compressive stresses stabilize

(2) After rainfall, a large amount of groundwater is replenished, and the swelling rock absorbs water and expands; the tensile stress on the upper layer of the rebar was the greatest at the center of the invert with a maximum value of roughly 17.3 MPa. The stress on the lower layer generally increased continuously over time. The compressive stress was the greatest at the center of the invert with a maximum value of roughly 120 MPa

(3) The stress on the rebar in the tunnel invert is mainly related to two factors: the temperature and groundwater. As the temperature of the concrete increased and decreased, the differing expansion coefficients of concrete and steel and the bond with the concrete compressed or elongated the rebar. Groundwater determines the swelling force of swelling rock, and stress from the rock acted on the concrete of the invert, which was equivalent to a statically indeterminate structure under the jacking force. This damaged the invert by bending; the upper layer of the rebar was under tensile stress, while the lower layer was under compressive stress

(4) Major changes in the stress on the rebar were observed 2–6 days after rain. The maximum compressive stress on the lower rebar increased from 35.7 MPa to 106.5 MPa, and the stress on the upper rebar changed from a compressive stress of 2 MPa to a tensile stress of 17.3 MPa. In 5 days, the compressive stress increased threefold, and the tensile stress increased 9.5-fold. This indicates that the expansion of surrounding rock caused by groundwater replenishment was the main reason for the change in stress on the rebar for Fuchuan Tunnel

(5) The stresses on the upper and lower layers of rebar in the tunnel invert followed a Gaussian distribution after the forces stabilized

Data Availability

The data used to support the findings of this study are available from the corresponding author upon request.

Conflicts of Interest

The authors have no conflicts of interest to declare.

Acknowledgments

This work was supported by a Project of Shandong Province Higher Educational Science and Technology Program (No. J18KA194), Open Research Fund of Key Laboratory of Urban Underground Engineering of Ministry of Education (TUE2019-03), and National Key R&D Program of China (2018YFC1505300-2).

References

[1] T. B. Li, "Damage to mountain tunnels related to the Wenchuan earthquake and some suggestions for aseismic tunnel construction," *Bulletin of Engineering Geology and the Environment*, vol. 71, no. 2, pp. 297–308, 2012.

[2] K. Shimamoto, K. Yashiro, Y. Kojima, Y. Nakanishi, K. Tsukada, and T. Asakura, "Study on the heaving caused by shear failure of roadbed and its countermeasures in mountain tunnels," *Journal of Japan Society of Civil Engineers Ser F1*, vol. 69, no. 1, pp. 54–72, 2013.

[3] K. Shimamoto, K. Yashiro, Y. Kojima, K. Tsukada, and T. Asakura, "Study on floor heave and its countermeasures in mountain tunnels with consideration of the influence of construction," *Journal of Japan Society of Civil Engineers Ser F1*, vol. 69, no. 2, pp. 105–120, 2013.

[4] Z. S. Tan, Z. L. Li, and W. Tang, "Research on stress characteristics of segment structure during the construction of the large-diameter shield tunnel and cross-passage," *Symmetry*, vol. 12, no. 8, article 1246, 2020.

[5] Q. Fang, H. R. Song, and D. L. Zhang, "Complex variable analysis for stress distribution of an underwater tunnel in an elastic half plane," *International Journal for Numerical and Analytical Methods in Geomechanics*, vol. 39, no. 16, pp. 1821–1835, 2015.

[6] C. P. Zhang, X. Zhang, and Q. Fang, "Behaviors of existing twin subway tunnels due to new subway station excavation below in close vicinity," *Tunnelling and Underground Space Technology*, vol. 81, pp. 121–128, 2018.

[7] L. Yu, D. L. Zhang, Q. Fang, L. Q. Cao, T. Xu, and Q. Q. Li, "Surface settlement of subway station construction using pile-beam-arch approach," *Tunnelling and Underground Space Technology*, vol. 90, pp. 340–356, 2019.

[8] P. F. Li, K. Y. Chen, F. Wang, and Z. Li, "An upper-bound analytical model of blow-out for a shallow tunnel in sand considering the partial failure within the face," *Tunnelling and Underground Space Technology*, vol. 91, p. 102989, 2019.

[9] P. F. Li, F. Wang, L. F. Fan, H. D. Wang, and G. W. Ma, "Analytical scrutiny of loosening pressure on deep twin-tunnels in rock formations," *Tunnelling and Underground Space Technology*, vol. 83, pp. 373–380, 2019.

[10] Z. Wen, S. Jing, Y. Jiang et al., "Study of the fracture law of overlying strata under water based on the flow- stress-damage model," *Geofluids*, vol. 2019, Article ID 3161852, 12 pages, 2019.

[11] Z. Wen, X. Wang, Y. Tan, H. Zhang, W. Huang, and Q. Li, "A study of rockburst hazard evaluation method in coal mine," *Shock and Vibration*, vol. 2016, Article ID 8740868, 9 pages, 2016.

[12] Z. Wen, E. Xing, S. Shi, and Y. Jiang, "Overlying strata structural modeling and support applicability analysis for large mining-height stopes," *Journal of Loss Prevention in the Process Industries*, vol. 57, pp. 94–100, 2019.

[13] Z. Li, H. Liu, Z. Dun, L. Ren, and J. Fang, "Grouting effect on rock fracture using shear and seepage assessment," *Construction and Building Materials*, vol. 242, article 118131, 2020.

[14] Z. Li, H. Zhou, D. Hu, and C. Zhang, "Yield criterion for rock-like geomaterials based on strain energy and CMP model," *International Journal of Geomechanics*, vol. 20, no. 3, article 04020013, 2020.

[15] Z. Li, S. Liu, W. Ren, J. Fang, Q. Zhu, and Z. Dun, "Multiscale laboratory study and numerical analysis of water-weakening effect on shale," *Advances in Materials Science and Engineering*, vol. 2020, Article ID 5263431, 14 pages, 2020.

[16] B. Chiaia, A. P. Fantilli, and P. Vallini, "Evaluation of crack width in FRC structures and application to tunnel linings," *Materials and Structures*, vol. 42, no. 3, pp. 339–351, 2009.

[17] A. Kaya and F. Bulut, "Geotechnical studies and primary support design for a highway tunnel: a case study in Turkey," *Bulletin of Engineering Geology & the Environment*, vol. 78, no. 8, pp. 6311–6334, 2019.

[18] X. Hu, Y. Fang, G. Walton, and C. He, "Experimental analysis of shield TBM tunnel lining mechanical behaviour in an anisotropically-jointed rock mass," *KSCE Journal of Civil Engineering*, vol. 23, no. 6, pp. 2733–2745, 2019.

[19] J. U. Yoon, J. W. Han, E. J. Joo, and J. H. Shin, "Effects of tunnel shapes in structural and hydraulic interaction," *KSCE Journal of Civil Engineering*, vol. 18, no. 3, pp. 735–741, 2014.

[20] M. Nematollahi and D. Dias, "Interaction between an underground parking and twin tunnels - case of the Shiraz subway line," *Tunnelling and Underground Space Technology*, vol. 95, p. 103150, 2020.

[21] A. Nogales and A. de la Fuente, "Crack width design approach for fibre reinforced concrete tunnel segments for TBM thrust loads," *Tunnelling and Underground Space Technology*, vol. 98, p. 103342, 2020.

[22] M. Bakhshi and V. Nasri, "Developments in design for fibre-reinforced concrete tunnel segments," in *Fibre-reinforced concrete: From design to structural applications - FRC 2014: ACI-fib international workshop*, July 2014.

[23] Q. X. Meng, H. L. Wang, M. Cai, W. Y. Xu, X. Y. Zhuang, and T. Rabczuk, "Three-dimensional mesoscale computational modeling of soil-rock mixtures with concave particles," *Engineering Geology*, vol. 277, article 105802, 2020.

[24] Q. X. Meng and W. Wang, "A novel closed-form solution for circular openings in generalized Hoek-Brown media," *Mathematical Problems in Engineering*, vol. 2014, Article ID 870835, 7 pages, 2014.

[25] Q. X. Meng, L. Yan, Y. L. Chen, and Q. Zhang, "Generation of numerical models of anisotropic columnar jointed rock mass

using modified centroidal Voronoi diagrams," *Symmetry*, vol. 10, no. 11, p. 618, 2018.

[26] B. Mou, F. Zhao, Q. Y. Qiao et al., "Flexural behavior of beam to column joints with or without an overlying concrete slab," *Engineering Structures*, vol. 199, no. 11, p. 109616, 2019.

[27] B. Mou, X. Li, Q. Y. Qiao, B. J. He, and M. L. Wu, "Seismic behaviour of the corner joints of a frame under biaxial cyclic loading," *Engineering Structures*, vol. 196, no. 10, p. 109316, 2019.

[28] K. Uenishi, "Elastodynamic analysis of underground structural failures induced by seismic body waves," *Journal of Applied Mechanics*, vol. 79, no. 3, article 031014, 2012.

[29] X. Y. Lv, Z. W. Yu, Z. Shan, and J. Yuan, "A stochastic damage model for bond stress-slip relationship of rebar-concrete interface under monotonic loading," *Materials*, vol. 12, no. 19, article 3151, 2019.

[30] L. Huang, H. L. Ye, S. H. Chu, and L. H. Xu, "Stochastic damage model for bond stress-slip relationship of reinforcing bar embedded in concrete," *Engineering Structures*, vol. 194, pp. 11–25, 2019.

[31] H. W. Lin, Y. X. Zhao, J. Ozbolt, and R. Hans-Wolf, "The bond behavior between concrete and corroded steel bar under repeated loading," *Engineering Structures*, vol. 140, pp. 390–405, 2017.

[32] G. Campione, C. Cucchiara, L. la Mendol, and M. Papia, "Steel-concrete bond in lightweight fiber reinforced concrete under monotonic and cyclic actions," *Engineering Structures*, vol. 27, no. 6, pp. 881–890, 2005.

[33] J. Z. Xiao, P. S. Li, and W. Qin, "Study on bond-slip between recycled concrete and rebar," *Journal of Tongji University*, vol. 34, no. 1, pp. 13–16, 2006.

[34] B. Wang, G. L. Bai, H. J. Dai, and S. H. Wu, "Experimental and mechanical analysis of bond-slip performance between recycled concrete and rebar," *Engineering Mechanics*, vol. 30, no. 10, pp. 54–64, 2013.

[35] C. Zhu, M. C. He, M. Karakus, X. B. Cui, and Z. G. Tao, "Investigating toppling failure mechanism of anti-dip layered slope due to excavation by physical modelling," *Rock Mechanics and Rock Engineering*, vol. 53, no. 11, pp. 5029–5050, 2020.

[36] X. J. Yang, J. M. Wang, D. G. Hou, C. Zhu, and M. C. He, "Effect of dry-wet cycling on the mechanical properties of rocks: a laboratory-scale experimental study," *Processes*, vol. 6, no. 10, p. 199, 2018.

[37] Z. Tao, C. Zhu, X. Zheng et al., "Failure mechanisms of soft rock roadways in steeply inclined layered rock formations," *Geomatics, Natural Hazards and Risk*, vol. 9, no. 1, pp. 1186–1206, 2018.

[38] Z. Tao, Z. Zhu, W. Han et al., "Static tension test and the finite element analysis of constant resistance and large deformation anchor cable," *Advances in Mechanical Engineering*, vol. 10, no. 12, Article ID 168781401881063, 2018.

[39] C. Zhu, X. Xu, W. Liu et al., "Softening damage analysis of gypsum rock with water immersion time based on laboratory experiment," *IEEE Access*, vol. 7, pp. 125575–125585, 2019.

[40] W. J. Zhang, W. T. Li, N. Yang, Q. Wang, T. C. Li, and G. Wang, "Determination of the bearing capacity of a concrete-filled steel tubular arch support for tunnel engineering: experimental and theoretical studies," *KSCE Journal of Civil Engineering*, vol. 21, no. 7, pp. 2932–2945, 2017.

[41] K. J. Kim, S. Y. Koh, S. Y. Choo, C. S. Hong, and D. J. Hwang, "A study of the invert tunnel's behavior in a weathered-rock using laboratory model test and numerical analysis," *ITA-AITES World Tunnel Congress and 33th General Assembly, 5–10*, Taylor and Francis/ Balkema, 2007.

[42] S. Seki, S. Kaise, Y. Morisaki, S. Azetaka, and Y. J. Jiang, "Model experiments for examining heaving phenomenon in tunnels," *Tunnelling and Underground Space Technology*, vol. 23, no. 2, pp. 128–138, 2008.

[43] M. Q. Du, X. C. Wang, Y. J. Zhang, L. Li, and P. Zhang, "In-situ monitoring and analysis of tunnel floor heave process," *Engineering Failure Analysis*, vol. 109, p. 104323, 2020.

[44] D. Mingqing, S. Jie, W. Xuchun, Z. Sulei, and Z. Yongjun, "Dynamic response and crack propagation law of tunnel invert with initial damage," *Engineering Failure Analysis*, vol. 119, article 104939, 2021.

[45] S. B. Tang and C. A. Tang, "Numerical studies on tunnel floor heave in swelling ground under humid conditions," *International Journal of Rock Mechanics and Mining Sciences*, vol. 55, pp. 139–150, 2012.

[46] Y. Wang, B. G. Liu, and Y. Qi, "A risk evaluation method with an improved scale for tunnel engineering," *Arabian Journal for Science and Engineering*, vol. 43, no. 4, pp. 2053–2067, 2018.

[47] F. K. Xiao, C. J. Zhang, L. W. Gao, and Y. Y. Yue, "Numerical research on the floor heave control of deep roadway in coal mining," *Advanced Materials Research*, vol. 524, pp. 446–449, 2012.